Research Article | Vol. 6, No. 12 | 1 Dec 2016 | OPTICAL MATERIALS EXPRESS 3927

Optical Materials EXPRESS

High-power passively continuous-wave and Q-switching mode-locked Nd:$LuVO_4$ laser by few-layer graphene-oxide films

Hou-Ren Chen,[1,*] Chih-Ya Tsai,[2] Hsin-Ming Cheng,[3] Kuei-Huei Lin,[4] Chyong-Hua Chen,[1] and Wen-Feng Hsieh[1]

[1]*Department of Photonics and Institute of Electro-Optical Engineering, National Chiao Tung University, 1001, Ta-Hsueh Rd., Hsinchu, 30010, Taiwan*
[2]*Department of Electrophysics, National Chiao Tung University, Hsinchu 300, Taiwan*
[3]*Material and Chemical Research Laboratories, Industrial Technology Research Institute, Hsinchu 310, Taiwan*
[4]*Department of Applied Physics and Chemistry, University of Taipei, 1, Ai-Guo West Rd., Taipei 100, Taiwan.*
**eittocs730318@g2.nctu.edu.tw*

Abstract: Using a series of different concentration polymer-free graphene oxide (GO) films as saturable absorbers (SAs), we demonstrate high-power passively continuous-wave mode-locking (CW-ML) and Q-switching mode-locking (QS-ML) for a Nd:$LuVO_4$ laser at 1 μm. CW-ML pulses of 6.62 ps with maximum output power of 3.89 W have been achieved to give the highest pulse peak power of 4.85 kW and pulse energy of 32.14 nJ under 15-W pumping by using SAs of 84.4% transmittance. Using SAs with a lower transmittance having a larger modulation depth of 75.9% and 63.4%, we obtain both the CW-ML pulses of 4.85-ps and QS-ML pulses with 2.73 W and 1.92 W output powers, respectively.

OCIS codes: (140.4050) Mode-locked lasers; (130.4310) Nonlinear; (160.4330) Nonlinear optical materials; (140.3580) Lasers, solid-state; (160.4236) Nanomaterials.

References and links

1. U. Keller, "Recent developments in compact ultrafast lasers," Nature **424**(6950), 831–838 (2003).
2. H. R. Chen, J. H. Lin, K. T. Song, K. H. Lin, and W. F. Hsieh, "Passive mode-locking in diode-pumped c-cut Nd:$LuVO_4$ laser with a semiconductor saturable-absorber mirror," Appl. Phys. B **96**, 19–23 (2009).
3. H. R. Chen, Y. G. Wang, C. Y. Tsai, K. H. Lin, T. Y. Chang, J. Tang, and W. F. Hsieh, "High-power, passively mode-locked Nd:$GdVO_4$ laser using single-walled carbon nanotubes as saturable absorber," Opt. Lett. **36**(7), 1284–1286 (2011).
4. H. R. Chen, C. Y. Tsai, H. M. Cheng, K. H. Lin, and W. F. Hsieh, "Passive mode locking of ytterbium- and erbium-doped all-fiber lasers using graphene oxide saturable absorbers," Opt. Express **22**(11), 12880–12889 (2014).
5. H. R. Chen, C. Y. Tsai, C. Y. Chang, K. H. Lin, C. S. Chang, and W. F. Hsieh, "Investigation of graphene dispersion from Kelly sideband in stable mode-locked Erbium-doped fiber laser by few-layer graphene saturable absorbers," J. Lightwave Technol. **33**, 4406–4412 (2015).
6. T. Hasan, Z. P. Sun, F. Q. Wang, F. Bonaccorso, P. H. Tan, A. G. Rozhin, and A. C. Ferrari, "Nanotube-polymer composites for ultrafast photonics," Adv. Mater. **21**, 3874–3899 (2009).
7. R. Mary, G. Brown, S. J. Beecher, F. Torrisi, S. Milana, D. Popa, T. Hasan, Z. Sun, E. Lidorikis, S. Ohara, A. C. Ferrari, and A. K. Kar, "1.5 GHz picosecond pulse generation from a monolithic waveguide laser with a graphene-film saturable output coupler," Opt. Express **21**(7), 7943–7950 (2013).
8. Z. P. Sun, D. Popa, T. Hasan, F. Torrisi, F. Q. Wang, E. J. R. Kelleher, J. C. Travers, V. Nicolosi, and A. C. Ferrari, "A stable, wideband tunable, near transform-limited, graphene-mode-locked, ultrafast laser," Nano Res. **3**, 653–660 (2010).
9. A. A. Lagatsky, Z. Sun, T. S. Kulmala, R. S. Sundaram, S. Milana, F. Torrisi, O. L. Antipov, Y. Lee, J. H. Ahn, C. T. A. Brown, W. Sibbett, and A. C. Ferrari, "2 μm solid-state laser mode-locked by single-layer graphene," Appl. Phys. Lett. **102**, 013113 (2013).
10. M. N. Cizmeciyan, J. W. Kim, S. Bae, B. H. Hong, F. Rotermund, and A. Sennaroglu, "Graphene mode-locked femtosecond Cr:ZnSe laser at 2500 nm," Opt. Lett. **38**(3), 341–343 (2013).
11. B. Fu, Y. Hua, X. S. Xiao, H. W. Zhu, Z. P. Sun, and C. X. Yang, "Broadband graphene saturable absorber for pulsed fiber lasers at 1, 1.5, and 2 μm," IEEE J. Sel. Top Quant. **20**, 1100705 (2014).

#278830 http://dx.doi.org/10.1364/OME.6.003927
Journal © 2016 Received 17 Oct 2016; revised 11 Nov 2016; accepted 21 Nov 2016; published 23 Nov 2016

Optical Materials EXPRESS

12. Q. L. Bao, H. Zhang, Y. Wang, Z. H. Ni, Y. L. Yan, Z. X. Shen, K. P. Loh, and D. Y. Tang, "Atomic-layer graphene as a saturable absorber for ultrafast pulsed lasers," Adv. Funct. Mater. **19**, 3077–3083 (2009).
13. G. Sobon, J. Sotor, I. Pasternak, A. Krajewska, W. Strupinski, and K. M. Abramski, "Multilayer graphene-based saturable absorbers with scalable modulation depth for mode-locked Er- and Tm-doped fiber lasers," Opt. Mater. Express **5**, 2884–2894 (2015).
14. L. F. Li, X. L. Zheng, X. M. Chen, M. Qi, Z. Y. Ren, J. T. Bai, and Z. P. Sun, "High-power diode-side-pumped Nd:YAG solid laser mode-locked by CVD graphene," Opt. Commun. **315**, 204–207 (2014).
15. J. L. Xu, X. L. Li, Y. Z. Wu, X. P. Hao, J. L. He, and K. J. Yang, "Graphene saturable absorber mirror for ultra-fast-pulse solid-state laser," Opt. Lett. **36**(10), 1948–1950 (2011).
16. W. D. Tan, C. Y. Su, R. J. Knize, G. Q. Xie, L. J. Li, and D. Y. Tang, "Mode locking of ceramic Nd:yttrium aluminum garnet with graphene as a saturable absorber," Appl. Phys. Lett. **96**, 031106 (2010).
17. J. Xu, J. Liu, S. Wu, Q. H. Yang, and P. Wang, "Graphene oxide mode-locked femtosecond erbium-doped fiber lasers," Opt. Express **20**(14), 15474–15480 (2012).
18. G. Sobon, J. Sotor, J. Jagiello, R. Kozinski, M. Zdrojek, M. Holdynski, P. Paletko, J. Boguslawski, L. Lipinska, and K. M. Abramski, "Graphene Oxide vs. Reduced Graphene Oxide as saturable absorbers for Er-doped passively mode-locked fiber laser," Opt. Express **20**(17), 19463–19473 (2012).
19. X. Li, K. Wu, Z. Sun, B. Meng, Y. Wang, Y. Wang, X. Yu, X. Yu, Y. Zhang, P. P. Shum, and Q. J. Wang, "Single-wall carbon nanotubes and graphene oxide-based saturable absorbers for low phase noise mode-locked fiber lasers," Sci. Rep. **6**, 25266 (2016).
20. C. Feng, Y. G. Wang, J. Liu, Y. H. Tsang, Y. R. Song, and Z. H. Yu, "3 W high-power laser passively mode-locked by graphene oxide saturable absorber," Opt. Commun. **298**, 168–170 (2013).
21. Y. G. Wang, H. R. Chen, X. M. Wen, W. F. Hsieh, and J. Tang, "A highly efficient graphene oxide absorber for Q-switched Nd:$GdVO_4$ lasers," Nanotechnology **22**(45), 455203 (2011).
22. Y. G. Wang, Z. S. Qu, J. Liu, and Y. H. Tsang, "Graphene oxide absorbers for watt-level high-power passive mode-locked Nd:$GdVO_4$ laser operating at 1 μm," J. Lightwave Technol. **30**, 3259–3262 (2012).
23. Y. G. Wang, H. R. Chen, W. F. Hsieh, and Y. H. Tsang, "Mode-locked Nd: $GdVO_4$ laser with graphene oxide/polyvinyl alcohol composite material absorber as well as an output coupler," Opt. Commun. **289**, 119–122 (2013).
24. L. Zhang, Y. G. Wang, H. J. Yu, S. B. Zhang, W. Hou, X. C. Lin, and J. M. Li, "High power passively mode-locked Nd:YVO_4 laser using graphene oxide as a saturable absorber," Laser Phys. **21**, 2072–2075 (2011).
25. X. Li, Y. L. Tang, Z. Y. Yan, Y. Wang, B. Meng, G. Z. Liang, H. D. Sun, X. Yu, Y. Zhang, X. P. Cheng, and Q. J. Wang, "Broadband saturable absorption of graphene oxide thin film and its application in pulsed fiber lasers," IEEE J. Sel. Top Quant. **20**, 1101107 (2014).
26. D. Mao, B. Q. Jiang, X. T. Gan, C. J. Ma, Y. Chen, C. J. Zhao, H. Zhang, J. B. Zheng, and J. L. Zhao, "Soliton fiber laser mode locked with two types of film-based Bi_2Te_3 saturable absorbers," Photonics Res. **3**, A43–A46 (2015).
27. J. Boguslawski, G. Sobon, R. Zybala, and J. Sotor, "Dissipative soliton generation in Er-doped fiber laser mode-locked by Sb_2Te_3 topological insulator," Opt. Lett. **40**(12), 2786–2789 (2015).
28. K. Yin, B. Zhang, L. Li, T. Jiang, X. F. Zhou, and J. Hou, "Soliton mode-locked fiber laser based on topological insulator Bi_2Te_3 nanosheets at 2 μm," Photonics Res. **3**, 72–76 (2015).
29. R. I. Woodward, R. C. T. Howe, G. Hu, F. Torrisi, M. Zhang, T. Hasan, and E. J. R. Kelleher, "Few-layer MoS_2 saturable absorbers for short-pulse laser technology: current status and future perspectives [Invited]," Photonics Res. **3**, A30–A42 (2015).
30. D. Mao, Y. Wang, C. Ma, L. Han, B. Jiang, X. Gan, S. Hua, W. Zhang, T. Mei, and J. Zhao, "WS_2 mode-locked ultrafast fiber laser," Sci. Rep. **5**, 7965 (2015).
31. S. X. Wang, H. H. Yu, and H. J. Zhang, "Band-gap modulation of two-dimensional saturable absorbers for solid-state lasers," Photonics Res. **3**, A10–A20 (2015).
32. C. Feng, X. Y. Zhang, J. Wang, Z. J. Liu, Z. H. Cong, H. Rao, Q. P. Wang, and J. X. Fang, "Passively mode-locked Nd^{3+}:YVO_4 laser using a molybdenum disulfide as saturable absorber," Opt. Mater. Express **6**, 1358–1366 (2016).
33. S. B. Lu, L. L. Miao, Z. N. Guo, X. Qi, C. J. Zhao, H. Zhang, S. C. Wen, D. Y. Tang, and D. Y. Fan, "Broadband nonlinear optical response in multi-layer black phosphorus: an emerging infrared and mid-infrared optical material," Opt. Express **23**(9), 11183–11194 (2015).
34. Z. Qin, G. Xie, C. Zhao, S. Wen, P. Yuan, and L. Qian, "Mid-infrared mode-locked pulse generation with multilayer black phosphorus as saturable absorber," Opt. Lett. **41**(1), 56–59 (2016).
35. J. Sotor, G. Sobon, W. Macherzynski, P. Paletko, and K. M. Abramski, "Black phosphorus saturable absorber for ultrashort pulse generation," Appl. Phys. Lett. **107**, 051108 (2015).
36. B. Zhang, F. Lou, R. Zhao, J. He, J. Li, X. Su, J. Ning, and K. Yang, "Exfoliated layers of black phosphorus as saturable absorber for ultrafast solid-state laser," Opt. Lett. **40**(16), 3691–3694 (2015).
37. X. Zhao, Z. B. Liu, W. B. Yan, Y. P. Wu, X. L. Zhang, Y. S. Chen, and J. G. Tian, "Ultrafast carrier dynamics and saturable absorption of solution-processable few-layered graphene oxide," Appl. Phys. Lett. **98**, 121905 (2011).
38. H. Zhang, S. B. Lu, J. Zheng, J. Du, S. C. Wen, D. Y. Tang, and K. P. Loh, "Molybdenum disulfide (MoS_2) as a broadband saturable absorber for ultra-fast photonics," Opt. Express **22**(6), 7249–7260 (2014).

Optical Materials EXPRESS

39. S. Lu, C. Zhao, Y. Zou, S. Chen, Y. Chen, Y. Li, H. Zhang, S. Wen, and D. Tang, "Third order nonlinear optical property of Bi_2Se_3," Opt. Express **21**(2), 2072–2082 (2013).
40. M. Z. Hasan and C. L. Kane, "Colloquium: Topological insulators," Rev. Mod. Phys. **82**, 3045–3067 (2010).
41. G. H. Zhang, H. J. Qin, J. Teng, J. D. Guo, Q. L. Guo, X. Dai, Z. Fang, and K. H. Wu, "Quintuple-layer epitaxy of thin films of topological insulator Bi_2Se_3," Appl. Phys. Lett. **95**, 053114 (2009).
42. C. J. Zhao, H. Zhang, X. Qi, Y. Chen, Z. T. Wang, S. C. Wen, and D. Y. Tang, "Ultra-short pulse generation by a topological insulator based saturable absorber," Appl. Phys. Lett. **101**, 211106 (2012).
43. C. Zhao, Y. Zou, Y. Chen, Z. Wang, S. Lu, H. Zhang, S. Wen, and D. Tang, "Wavelength-tunable picosecond soliton fiber laser with Topological Insulator: Bi_2Se_3 as a mode locker," Opt. Express **20**(25), 27888–27895 (2012).
44. S. Q. Chen, Y. Chen, M. Wu, Y. Li, C. J. Zhao, and S. C. Wen, "Stable Q-switched Erbium-doped fiber laser based on Topological Insulator covered microfiber," IEEE Photonic Tech. L. **26**, 987 (2014).
45. Z. C. Luo, M. Liu, H. Liu, X. W. Zheng, A. P. Luo, C. J. Zhao, H. Zhang, S. C. Wen, and W. C. Xu, "2 GHz passively harmonic mode-locked fiber laser by a microfiber-based topological insulator saturable absorber," Opt. Lett. **38**(24), 5212–5215 (2013).
46. F. Bonaccorso and Z. P. Sun, "Solution processing of graphene, topological insulators and other 2d crystals for ultrafast photonics," Opt. Mater. Express **4**, 63–78 (2014).
47. R. I. Woodward, E. J. R. Kelleher, R. C. T. Howe, G. Hu, F. Torrisi, T. Hasan, S. V. Popov, and J. R. Taylor, "Tunable Q-switched fiber laser based on saturable edge-state absorption in few-layer molybdenum disulfide (MoS_2)," Opt. Express **22**(25), 31113–31122 (2014).
48. Y. Cai, G. Zhang, and Y. W. Zhang, "Layer-dependent band alignment and work function of few-layer phosphorene," Sci. Rep. **4**, 6677 (2014).
49. D. Hanlon, C. Backes, E. Doherty, C. S. Cucinotta, N. C. Berner, C. Boland, K. Lee, A. Harvey, P. Lynch, Z. Gholamvand, S. Zhang, K. Wang, G. Moynihan, A. Pokle, Q. M. Ramasse, N. McEvoy, W. J. Blau, J. Wang, G. Abellan, F. Hauke, A. Hirsch, S. Sanvito, D. D. O'Regan, G. S. Duesberg, V. Nicolosi, and J. N. Coleman, "Liquid exfoliation of solvent-stabilized few-layer black phosphorus for applications beyond electronics," Nat. Commun. **6**, 8563 (2015).
50. Y. Shen, S. B. Yang, P. Zhou, Q. Q. Sun, P. F. Wang, L. Wan, J. Li, L. Y. Chen, X. B. Wang, S. J. Ding, and D. W. Zhang, "Evolution of the band-gap and optical properties of graphene oxide with controllable reduction level," Carbon **62**, 157–164 (2013).
51. C. Honninger, R. Paschotta, F. Morier-Genoud, M. Moser, and U. Keller, "Q-switching stability limits of continuous-wave passive mode locking," J. Opt. Soc. Am. B **16**, 46–56 (1999).
52. Z. Wang, H. Zhang, E. Xu, D. Hu, X. Xu, J. Wang, and Z. Shao, "High-power, continuous-wave, Nd:$LuVO_4$ microchip lasers," Laser Phys. Lett. **5**, 25–28 (2008).
53. J. C. Chiu, Y. F. Lan, C. M. Chang, X. Z. Chen, C. Y. Yeh, C. K. Lee, G. R. Lin, J. J. Lin, and W. H. Cheng, "Concentration effect of carbon nanotube based saturable absorber on stabilizing and shortening mode-locked pulse," Opt. Express **18**(4), 3592–3600 (2010).
54. V. C. Tung, M. J. Allen, Y. Yang, and R. B. Kaner, "High-throughput solution processing of large-scale graphene," Nat. Nanotechnol. **4**(1), 25–29 (2009).
55. W. S. Hummers, Jr. and R. E. Offeman, "preparation of graphitic oxide," J. Am. Chem. Soc. **80**, 1339 (1958).
56. H. C. Schniepp, J. L. Li, M. J. McAllister, H. Sai, M. Herrera-Alonso, D. H. Adamson, R. K. Prud'homme, R. Car, D. A. Saville, and I. A. Aksay, "Functionalized single graphene sheets derived from splitting graphite oxide," J. Phys. Chem. B **110**(17), 8535–8539 (2006).
57. G. Eda and M. Chhowalla, "Chemically derived graphene oxide: towards large-area thin-film electronics and optoelectronics," Adv. Mater. **22**(22), 2392–2415 (2010).
58. D. C. Marcano, D. V. Kosynkin, J. M. Berlin, A. Sinitskii, Z. Sun, A. Slesarev, L. B. Alemany, W. Lu, and J. M. Tour, "Improved synthesis of graphene oxide," ACS Nano **4**(8), 4806–4814 (2010).
59. L. Zhang, Y. G. Wang, H. J. Yu, W. Sun, Z. H. Han, S. B. Zhang, W. Hou, X. C. Lin, J. M. Li, and J. Tang, "Passively Q-switched and mode-locked Nd:YVO_4 laser with sandwich structured wallpaper graphene oxide absorber," Laser Phys. **22**, 133–136 (2012).
60. S. C. Xu, B. Y. Man, S. Z. Jiang, C. S. Chen, C. Yang, M. Liu, Q. J. Huang, C. Zhang, D. Bi, X. Meng, and F. Y. Liu, "Watt-level passively Q-switched mode-locked YVO_4/Nd:YVO_4 laser operating at 1.06 μm using graphene as a saturable absorber," Opt. Laser Technol. **56**, 393–397 (2014).
61. G. Wang, Q. Song, Y. Gao, B. Zhang, W. Wang, M. Wang, Q. Zhang, W. Liu, D. Sun, F. Peng, and G. Sun, "Passively Q-switched mode locking performance of Nd:$GdTaO_4$ crystal by MoS_2 saturable absorber at 1066 nm," Appl. Opt. **54**(18), 5829–5832 (2015).
62. P. X. Li, G. J. Zhang, H. Zhang, C. J. Zhao, J. J. Chi, Z. Q. Zhao, C. Yang, H. W. Hu, and Y. F. Yao, "Q-switched mode-locked Nd:YVO_4 laser by Topological insulator Bi_2Te_3 saturable absorber," IEEE Photonic Tech. L. **26**, 1912–1915 (2014).

1. Introduction

Various continuous wave mode-locking (CW-ML) techniques have been widely used in diode-pumped solid-state laser (DPSSL) to generate high peak power and ultra-short pulse lasers because of their wide-spreading applications in optical communication, medicine,

Optical Materials EXPRESS

micro-machining, and materials processing [1]. Passive ML pulses are usually obtained using materials with nonlinear absorption, in which saturable absorption plays an important role to generate ultrashort pulsed lasers [2–5]. Recently, the research on newly emerging saturable absorption materials primarily is focused on graphene [5–16], graphene oxides (GO) [4,17–25] and graphene-like two-dimensional (2D) materials such as topological insulators (TIs) [26–28], semiconducting transition-metal dichalcogenides (TMDCs) [29–32], and black phosphorus (BPs) [33–36]. Compared with the traditional semiconductor saturable absorber mirrors (SESAMs), these new nanomaterials like graphene and graphene-like 2D materials take the advantages of unique electronic band structure, broadband absorption, controllable modulation depth, ultrafast carrier dynamics, and large optical nonlinearity [12, 33, 37–39]. Therefore, these new nanomaterials have the potential to be used as broadband SAs for laser mode-locking. However, graphene has a small absorption of only 2.3% and a low differential transmittance ΔT (or low modulation depth) of ~0.75% at 1060 nm. The small ΔT might not be enough to suppress CW components to obtain mode-locked pulses in high gain laser systems (e.g., Yb-doped fiber laser system). Although Chen et al. [5] and Sobon et al. [13] directly grew the multilayer graphene and stacked single-layer graphene to form different number of layers, respectively, in order to enhance the ΔT, it is still very difficult in controlling the layer numbers of graphene. The more complex preparation process and large-scale production of high-quality TI films [40, 41] limit their applications in photonics and optoelectronics. Recently, the TI nanomaterials which had high absolute ΔT up to 90% [42, 43] were manufactured using wet chemical synthesis method (e.g., polyol method [42, 43] and hydrothermal intercalation with liquid phase exfoliation method [44–46]). However, they weren't water soluble, which limited the flexibility and processibility for large-scale production of TI-based optoelectronics. For the semiconductor TMDCs, the wideband sub-bandgap (near-IR range) saturable absorption was attributed to energy levels within the bandgap (monolayer MoS_2: direct bandgap of 1.86 eV) arising from edge state [47], however, the amount of edge states weren't easy to control. Whereas, BPs is a direct bandgap semiconductor in the mono-, few-layers, and bulk form. Its bandgap depends on the number of layers and decreases with increasing thickness, ranging from 0.3 eV (mono-BPs) to 1.5 eV (bulk BPs) [48]. However, fabrication process of the BPs nanomaterials must be in an argon-filled glove box to avoid degrading rapidly by introduction of water and O_2 [49].

GO is the precursor for reduced GO (rGO), which can be fabricated by strong oxidization inexpensive graphite as raw material, and then exfoliating the graphite oxide in water through sonication. Compared with graphene, GO is highly hydrophilic due to the presence of oxygen-containing functional groups and can form stable aqueous colloids to facilitate the assembly of macroscopic structures by simple and low-cost solution processes. Although the oxygen functional groups destroy the gapless linear dispersion of Dirac electrons in graphene and make the GO insulating, the GO still possesses almost constant absorbance from 0.8 to 2.5 μm [50]. In addition, Sobon et al. [18] have demonstrated that there is no significant difference in the laser performance between the GO- and rGO-based SAs. Taking into account the simpler manufacturing technology and the possibility of mass production, GO seems to be a good candidate as a cost-effective material for SAs for mode-locked lasers. Although Feng et al. [20] has achieved mode-locked Nd:YVO_4 laser with a maximal output power of 3.06 W by reflective graphene oxide saturable absorber (GOSA), the pulse duration is 8.8 ps, However, the output optical path isn't collinear in this result (i.e., the total power of two output beams with a certain angle is 3W). Wang et al. [22] generated 4.5-ps mode-locked Nd:$GdVO_4$ laser by using a GOSA with ΔT of 12%; however, the maximum output is only 1.1 W. In addition, both of these two reports used the complex five-mirror cavity setup in order to reduce the repetition rate (or increase pulse energy) of mode-locked pulses due to large ΔT of GOSAs. From stable CW-ML condition, it is required that the intra-cavity pulse energy E_p goes beyond a threshold against the Q-switching instability [3, 51]. We choose Nd:$LuVO_4$ as the laser gain medium to prevent Q-switching instability, because its emission

Optical Materials EXPRESS

cross section (14.6 x 10^{-19} cm^2) is larger than those of the Nd:$GdVO_4$ (7.6 x 10^{-19} cm^2) and Nd:YVO_4 (13.5 x 10^{-19} cm^2) gain media [2]. In addition, the Nd:$LuVO_4$ crystal have the larger damage threshold and the absorption cross section than other three Nd-doped crystals. Therefore, it has been demonstrated for achieving high laser power and efficiency [52].

In this paper, we fabricate a series of polymer-free GO films incorporating different amounts of GO by using a vertical evaporation technique onto a quartz substrate [3], and present a systematic study on Nd:$LuVO_4$ laser characteristics by using GOSAs. The ΔT of GOSA is tunable by changing the GO concentration [53] due to its water solubility. In use of a GOSA under 15-W pumping, an Nd:$LuVO_4$ mode-locked laser with simpler 4-mirror cavity setup operated at 1065.6 nm, maximal output power of 3.89 W has been achieved. The repetition rate is 121.2 MHz and the pulse duration is 6.62 ps. In addition, Nd:$LuVO_4$ laser operated in mode-locked state with the narrowest pulse duration of 4.85 ps and output power of 2.73 W, as well as widely pumping range for QS-ML state, have been achieved by using GOSAs with larger ΔT. To our knowledge, we obtain the highest output power of 3.89 W and 1.92 W for CW-ML and QS-ML pulses, respectively, in use of GOSAs.

2. GO flakes preparation and characterization

The GO flakes used in this experiment were prepared through a modified Hummers method [54, 55] from expanded acid-washed graphite flakes. Morphologies and sizes of the products were observed by a field-emission scanning electron microscope (JEOL JSM-6500F). The surface topology and thickness of GO flakes were determined by an atomic force microscope (SEIKO SPA-300) with a tapping mode. The sample was prepared by drop-casting the GO dispersion on the surface of the Si substrate and then dried in vacuum drying oven. Figure 1(a) shows the SEM image of GO flakes, which exhibits the layered structure, and morphology resembles thin certainly, indicating very good exfoliation of graphite during oxidation process, and having mean diameter of 1~6 μm (scale bar 1 μm). 2D topographical image of GO nanomaterials could be clearly observed as shown in Fig. 1(b). For precisely analyzing the thickness of GO flakes, two different sections were chosen for the measurements, as marked in Fig. 1(b). Figures 1(c)-1(d) show the height variation between the two GO flakes sections. The heights of A, B, C, and D are 1.74, 2.57, 3.41, and 2.62 nm, respectively. Therefore, the height differences $H_{A\text{-}B}$, $H_{C\text{-}D}$ are about 0.83 and 0.79 nm, respectively, indicating near monolayer GO flakes [56].

Optical Materials EXPRESS

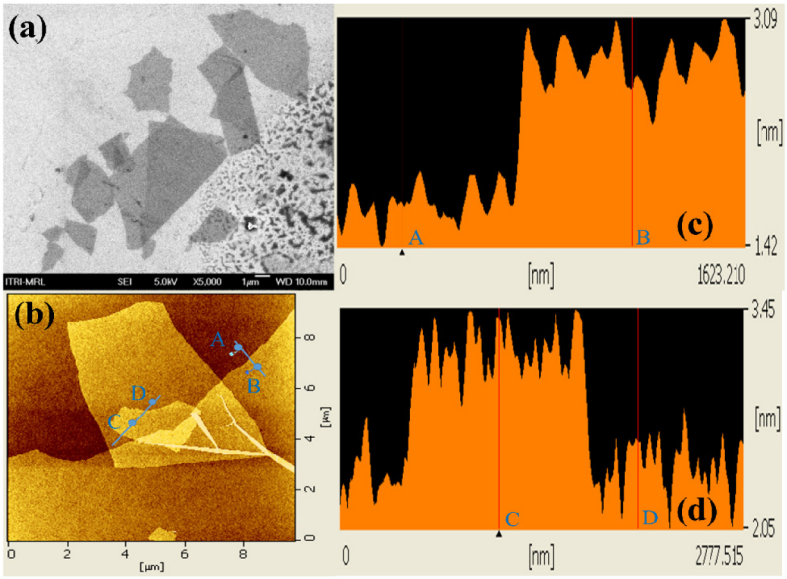

Fig. 1. (a) SEM image of GO flake; (b) 2D topographical AFM image of GO flake; (c) and (d) Height profiles of the sections marked in (b).

The Raman spectrum in Fig. 2(a) was obtained with a 532-nm laser excitation. The two prominent peaks at 1350 cm^{-1} and 1589 cm^{-1} are assigned to the D and G bands, respectively. The D peak is due to the defect-induced breathing mode of sp^2 rings. The G peak corresponds to optical E_{2g} photons at the Brillouin zone center and is due to bond stretching of sp^2 carbon pairs in both rings and chains [57]. The structure of the GO flakes is characterized by X-ray diffraction (XRD) 2θ-ω scans using a PANalytical Empyrean X-ray diffractometer (Cu $K_{\alpha 1}$, λ = 1.54056 Å) to examine the out-of-plane orientation as shown in Fig. 2(b). The GO exhibits a sharp peak at 2θ = 10.4°, corresponding to the interlayer spacing of 0.85 nm calculated via the Bragg equation, indicating the presence of oxygen-containing functional groups in interlayer spaces after oxidation. The measured GO thickness of 0.85 nm using AFM is consistent with XRD results. These groups enlarge the interlayer spacing between GO sheets to 0.85 nm from 0.34 nm [58]. In addition, there is very weak but broad peak at around 21° (red rectangle), indicating that almost no disordered component was generated during the chemical processing of graphite to make the GO flakes.

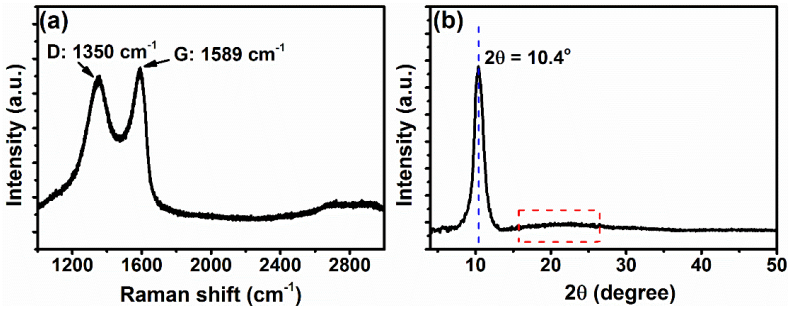

Fig. 2. (a) Raman spectrum and (b) XRD pattern of GO flakes.

Optical Materials EXPRESS

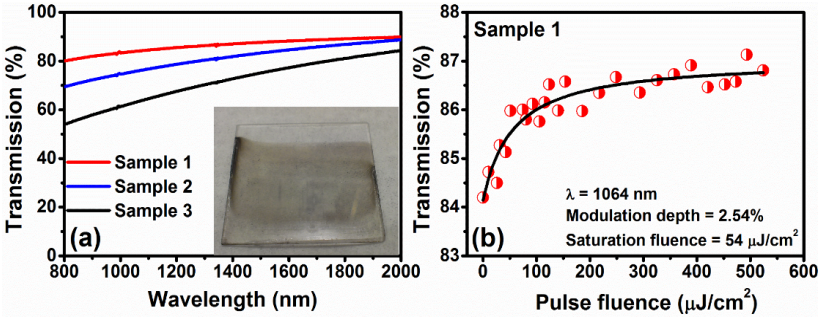

Fig. 3. (a) Optical transmission spectra of GOSA films incorporating different amounts of GO flakes. (b) Nonlinear transmission of the GOSAs with excitation wavelength at 1064 nm. Dots: measured data; solid curve: fitting to the data.

The polymer-free GOSAs (photograph shown in the inset of Fig. 3(a)) were the same thickness of about 15 μm, named as samples 1, 2 and 3, incorporating different amounts of 0.6-, 0.9-, and 1.25-mg GO powder, respectively. The detailed preparation of GOSAs are similar to Ref [3]. The transmission spectra of different concentration GOSAs are shown in Fig. 3(a), which were measured by a UV-visible-NIR spectrophotometer. The transmission spectra of GOSAs show monotonic increase in the spectral range from 350 to 2000 nm, which is a typical feature of GO and is similar to [4] and [18]. It might be caused by the oxygen-containing functional groups, which have larger absorption at short wavelength. The measured transmission (T_{1064}) of samples 1, 2, and 3 are 84.1%, 75.9%, and 63.4% at 1064 nm, respectively. The nonlinear transmittance and saturation fluence were measured by the pump-probe setup described in Ref [3]. The measured nonlinear transmission of sample A at 1064 nm is shown in Fig. 3(b). By fitting the absolute transmission of the GOSAs as a function of the input pulse fluence, we acquired the saturation fluence ($F_{sat,A}$), modulation depth (ΔT), and non-saturable loss. The detailed results were listed in Table 1. The $F_{sat,A}$, ranging from 54 to 57 μJ/cm^2, corresponds to the saturation intensity I_{sat} = 145 to 154 MW/cm^2 calculated from $I_{sat} = F_{sat,A}/\tau$, provided that the recovery time τ = 370 fs is used [37]. ΔT = 2.54%, 4.14%, and 5.36%, and non-saturable loss = 13.36%, 19.86%, and 31.24% for samples 1, 2, and 3, respectively. The measured $F_{sat,A}$ ~54 to 57 μJ/cm^2 is smaller than 80 μJ/cm^2 of Ref [22]. The $F_{sat,A}$ for SAs with different amount of GOs range from 0.6 to 1.25 mg were measured within 54 ~57 μJ/cm^2, indicating that high purity and well-dispersed GO samples are prepared.

Table 1. Linear and nonlinear optical properties of GOSAs at 1064 nm

	Sample 1	Sample 2	Sample 3
Linear transmission, T_{1064}	84.1%	75.9%	63.4%
Saturation fluence, $F_{sat,A}$	54 μJ/cm^2	57 μJ/cm^2	57.1 μJ/cm^2
Modulation depth, ΔT	2.54%	4.14%	5.36%
Non-saturable loss	13.36%	19.96%	31.24%

Optical Materials EXPRESS

3. Experimental setup of GO mode-locked Nd: $LuVO_4$ lasers

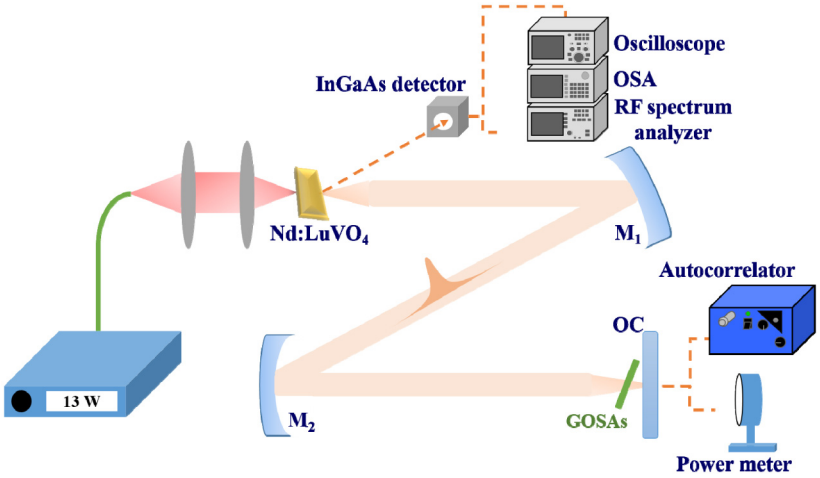

Fig. 4. Schematic setup of the passively ML and QS-ML *a*-cut Nd:$LuVO_4$ laser with the GOSAs. M_1 and M_2 are the folding mirrors and OC is the output coupler.

The schematic laser setup with Z-folded resonator is shown in Fig. 4. The fiber coupled diode array laser with central wavelength of 808 nm was used as the pump source. The pump beam from the fiber was imaged on a 3x3x8 mm^3 *a*-cut Nd:$LuVO_4$ crystal with 0.5-at.% Nd^{3+} concentration. The laser crystal was wrapped with indium foil and mounted in a water-cooled copper block, where the water temperature was maintained at 15°C to prevent unwanted high temperature from causing crystal damage and power fluctuation. One facet of the Nd:$LuVO_4$ crystal is high-reflection (HR) coated at 1064 nm and anti-reflection (AR) coated at 808 nm; and the other facet with 2 degree wedge is AR coated at 1064 nm. Two curved mirrors M_1 and M_2, which have radii of curvatures of 500 and 200 mm and HR coating at 1064 nm (R > 99.8%) were used as the folding mirrors to transmit cavity beam through the GO to the output coupler (OC). The reflectivity of the OC mirror is 82% coated at 1064 nm. The radius of the cavity mode at the gain medium was estimated to be ~200 μm using the ABCD law with consideration of the thermal lensing effect. The GOSA was mounted in the compact water-cooled copper block maintained at 15°C under N_2 flow, which was controlled by a mass flow controller. The GOSA was put close to the OC and mounted with Brewster angle to minimize the cavity loss. The beam radius at the GOSA was ~35 μm. Various GOSAs with concentration of 0.15, 0.3, and 0.6 mg for tuning the initial transmittance and modulation depth were used to optimize the generation of high-power CW-ML pulses. The output power of the Nd:$LuVO_4$ laser from OC was measured by a power meter (Ophir Inc.). The leakage light from the wedged crystal facet is detected and characterized by a high-speed InGaAs detector that was connected to the oscilloscope (LeCroy LT372) and 2.9-GHz radio-frequency (RF) spectrum analyzer (HP 8560E). The spectrum was measured by an optical spectrum analyzer (Ando AQ6315A). A non-collinear autocorrelator (FR-103WS) was used to measure the width of mode-locked pulses.

4. Results and discussion

Figure 5 shows the measured average laser output power as a function of the pump power for the CW state (without Polymer-free GOSAs, open black squares), the CW-ML states in use of sample 1 with T_0 = 84.1% (green stars) and sample 2 with 75.9% (red circles), as well as the QS-ML states in use of sample C with 63.4% (blue triangles). The threshold for CW lasing is 0.62 W and the slope efficiency is 38%. As expected, after the GOSAs were inserted into the laser cavity, the laser not only increases in CW lasing threshold but also eventually achieves

Optical Materials EXPRESS

the CW-ML state (solid symbols) through the intermediate irregular QS-ML state (open symbols) and regular QS-ML state (half-filled symbols) for samples 1 and 2. In ML DPSSLs by the SAs, the threshold for the CW-ML against the QS-ML can be reached as the intra-cavity energy exceeds the critical value E_p to prevent Q-switching instabilities according to $E_p > (F_{sat,L}A_L F_{sat,L}A_A\Delta T)^{1/2}$, where $F_{sat,L}$ and A_L are the saturation fluence and the laser effective area of the gain medium, respectively; $F_{sat,A}$ and A_A are those for the GOSAs. The $F_{sat,L}$ for the *a*-cut Nd:$LuVO_4$ laser is calculated to be about 0.064 J/cm^{-2} with the definition $F_{sat,L} = h\nu / m\sigma$ [51]. Here, $h\nu$ is the photon energy, m is 2 for the standing-wave cavity, and σ_L is the emission cross section. Sample 3 exhibit the largest ΔT, therefore there is the highest CW-ML threshold because it has the highest concentration among the three GOSAs. The ΔT of sample 3 is too large to overcome Q-switching instability in our available pumping power. Therefore, only QS-ML state is obtained at all range of pumping power up to 15.3 W. It is worth to mention that stable QS-ML state can be obtained with a wide pumping power ranging from 12.3 to 15.3 W (available pumping power). The maximal output power is 1.92 W under pump power of 15.3 W. Sample 2 has smaller ΔT than sample 3, therefore the threshold of CW-ML is lower than that in use of sample 3. As the pumping power is set 12.7 W, CW-ML is observed (calculated threshold pump power of CW-ML is 13.2 W), and the highest output power is about 2.73 W with the pump power of 15 W. Although the maximum QS-ML output power of 2.22 W with sample 2 is slightly larger than that with sample 3, the pump-power range for QS-ML operation is smaller. In order to obtain a much lower CW-ML threshold with higher output power, we have replaced sample 1 to sample 2 and acquired the lasing threshold of about 2.4 W with slope efficiency of 31.2%, and then the CW mode-locked pulses were obtained when the pump power is increased above 7 W (calculated CW-ML threshold is 7.8 W). A remarkable output power of 3.89 W was obtained in CW-ML regime under P_p = 15 W. The results are similar to Ref [3]. by using single-walled carbon nanotube, showing that GO can be used in high-power passively ML lasers.

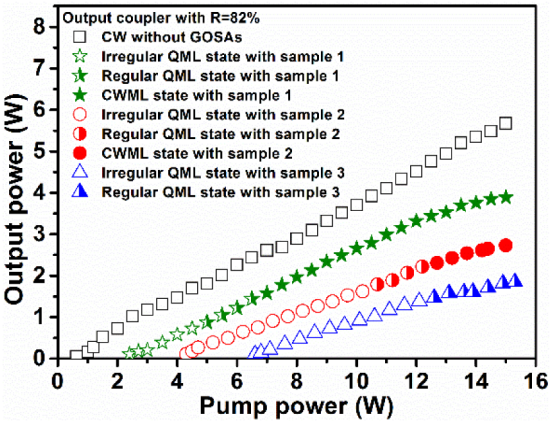

Fig. 5. Average output power versus pump power of the Nd:$LuVO_4$ laser for CW, QS-ML and ML operations with output coupling of 18%.

The time trace of mode-locked pulse trains, RF spectrum, optical spectrum, and pulse duration by using samples 1 and 2 under pump power of 15 W were recorded and shown in Figs. 6(a)-6(d). In the regular CW-ML pulse trains, the temporal separation between the pulses is about 8.25 ns (Fig. 6(a)), corresponding to 121.2 MHz repetition rate that agrees with the RF spectrum in the inset of Fig. 6(b). The long time scale pulse train at CW-ML state (inset of Fig. 6(a)) reveals that the CW-ML state is free from Q-switching modulation. For the fundamental beating at 121.2 MHz (Fig. 6(b)), we can observe a very high extinction ratio of 66.1 dB against the noise without any spurious modulations, which have demonstrated a very clean CW-ML operation of this Nd:$LuVO_4$ laser. The inset of Fig. 6(c) shows the spectrum of

Optical Materials EXPRESS

the ML pulses, whose central wavelength is 1065.6 nm and the bandwidth is 0.41 nm (full width at half maximum, FWHM). The autocorrelation trace of the output pulses is depicted in Fig. 6(c), and the pulse duration is about 6.62 ps (assuming a Gaussian pulse shape). The calculated time-bandwidth product (TBP) is 0.71, which is larger than the transform-limited value of 0.44 for Gaussian pulses, indicating that the mode-locked pulses are frequency chirped and their duration could be further narrowed by group dispersion compensation. While inserting sample 2 into the Nd:$LuVO_4$ laser, narrower pulse duration of about 4.85 ps can be obtained (Fig. 6(d)) under pump power of 15 W due to strong pulse shaping caused by the larger modulation depth of SAs. However, the maximal output power is only 2.73 W under P_p = 15 W, which is lower than that with sample 1, due to the larger non-saturable loss caused by large amount of GO. The central wavelength and FWHM of optical spectrum are 1065.7 nm and 0.436 nm, respectively (inset of Fig. 6(d)). The calculated TBP is 0.56. Using the measured average output power of 3.89 W, pulse repetition rate of 121.2 MHz, and pulse width of about 6.62 ps, we estimated the pulse energy and the peak power to be about 32.14 nJ and 4.85 kW, respectively, under the 15 W pump power. The polymer-free GOSAs have been demonstrated a good material for high-power passively ML lasers. Without the N_2 flow, the mode-locked laser can be operated for about 10-20 min. due to degradation by further oxidation. Nevertheless, the mode locking continues with the output power instability of about ± 3% for more than an hour with 40 SCCM N_2 purge to the GOSA. Under the limited 15 W pump power, we didn't observe damage of the GOSA under N_2 purge, indicating its damage threshold is higher than 810 MW/cm^2 which is higher than 348.6 MW/cm^2 for graphene-SAs in Ref [14].

Table 2 summarizes output performance of free space mode locked Nd-doped crystal lasers at 1 μm by graphene (G)-, GO-, TMDCs-, BPs- based SAs. The performance of ultrafast solid-state lasers mode-locked by GSAs and GOSAs have steadily improved. However, there is relatively few papers to obtain ML pulses by BPs- and TMDCs-SAs mainly because of the difficulty in fabrication and the need to improve their damage threshold. For example, Zhang et al. [36], reports the BPs based mode-locked Nd:YVO_4 solid state lasers. The BPs-SAs with linear transmittance of 82% have the modulation depth (ΔT), saturation intensity (I_{sat}), and nonsaturable loss of about 7.5%, 1.35 MW/cm^2, and 10.5%. It seems to be more efficiency in saturable absorption of light than our GOSAs samples having ΔT, $I_{sat,}$ and nonsaturable loss to be 2.54%, 145 MW/cm^2 (if the recovery time τ = 370 fs is used), and 13.36%, respectively, and almost same linear transmittance of 84.1%. However, there is only one reported BPs-based mode-locked Nd:YVO_4 solid state laser operated at 460 mW output under 3.61 W pumped power. It might be not suitable for high power bulk laser because of easy oxidation and deliquescence in air [33]. Therefore, it is necessary for BPs to cover an effective capping layer protecting BP from the structural and chemical degradation in ambient condition. Comparing to other reports, an Nd:$LuVO_4$ mode-locked laser by using GOSA with simpler 4-mirror cavity setup operated at 1065.6 nm, maximal output power of 3.89 W has been achieved. The repetition rate is 121.2 MHz and the pulse duration is 6.62 ps.

Table 2. Passively mode-locked solid state laser based on Nd doped crystals with graphene and graphene-like 2D materials SAs (G: graphene; GO: graphene oxide; BP: black phosphorus; T: transmissive type; R: reflective type; λ: center wavelength; τ: pulse width; P: output power; E_p: pulse energy; P_p: peak power.)

Laser type / SAs	Coupling method	Laser parameters						Ref.
		λ (nm)	τ (ps)	R_{ep} (MHz)	P (W)	E_p (nJ) / P_p (kW)	Slope efficiency	
Nd:YAG / G	T	1064	13	114	2.1	18.4 / 1.33	//	[14]
Nd:YAG / G	T	1064.4	4	88	0.1	1.1 / 0.28	//	[16]

Optical Materials EXPRESS

Nd:$GdVO_4$ / GO	T	1063	4.5	75	1.1	15.7 /3.5	11.3%	[22]
Nd:$GdVO_4$ / GO	T	1063	12	120	0.68	5.7 / 0.47	13%	[23]
Nd:$GdVO_4$ / G	T	1065	16	43	0.36	8.4 / 0.53	22.5%	[15]
Nd:YVO_4 / GO	T	//	//	88	1.2	13.6 / //	30%	[59]
Nd:YVO_4 / GO	R	1065.5	8.8	84	3.06	36 / 4.1	25%	[20]
Nd: YVO4 / BP	T	1064.1	6.1	142.8	0.46	3.29 / 0.54	14%	[36]
Nd:YVO_4 / MoS_2	T	1064.2	12.7	88.3	0.089	1 / 0.0833	4%	[32]
Nd: $LuVO_4$ / GO	T	1065.6	6.62	121.2	3.89	32.14 / 4.85	31.2%	This work

Figures 7(a)-7(b) show the stable regular QS-ML trains for pump power of 12.3 and 15.3 W, respectively by using sample 3. The repetition rate of QS envelope increases from 139 to 155 KHz, corresponding to time spacing of 7.19 to 6.45 μs, as the pump power increases from 12.3 W to 15.3 W. Figure 7(c) shows temporal profile of a single QS-ML envelope and the mode-locked pulse trains inside the QS-ML envelope under pump power of 15.3 W. By fitting the envelope with the bi-exponetial formula:

$$I(\mathrm{t}) = [\frac{I_0}{\exp(1.76\,\mathrm{t}/\,\mathrm{t}_1) + \exp(-1.76\,\mathrm{t}/\,\mathrm{t}_2)}]^2,$$

where I_0 is the scaling factor, the rising time t_1 = 0.47 μs and the falling time t_2 = 0.51 μs of the QS-ML envelopes can be obtained. The width of QS envelopes can be estimated by the definition of $\tau = (t_1 + t_2)/2$ = 0.49 μs. The repetition rate of mode-locked pulses inside the QS envelope is 121.2 MHz (inset of Fig. 7(c)), which is determined by the length of the laser cavity. The width of the individual mode-locked pulse inside QS envelope, measured by an autocorrelator (black squares), is about 175 ps by fitting to the Gaussian shape (red curve) as shown in Fig. 7(d). The maximal output power of QS-ML pulse is 1.92 W, which is larger than other reports on QS-ML by 2D materials such as 1.6 W by graphene [60], 156 mW by MoS_2 [61], 310 mW by GO [59], and 247 mW by Bi_2Te_3 [62]. At 15.3-W pump power, the peak power of QS-ML pulses calculated by $P_p = P_0/NR_{ep}t_0$ is 1.18 kW, where P_0 is the average output power, R_{ep} is the repetition rate of the QS envelope, N is the number of pulses within a QS envelope (assuming 60 pulses), and t_0 is the width of the ML pulses.

Optical Materials EXPRESS

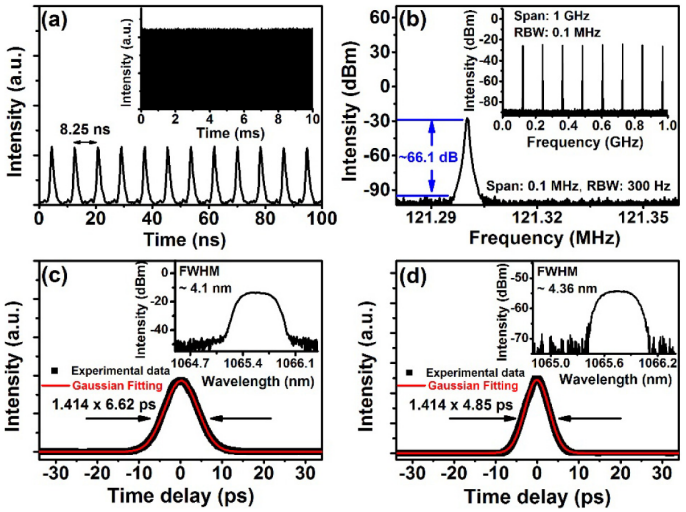

Fig. 6. (a) CW mode-locked pulse trains of the *a*-cut Nd:$LuVO_4$ laser on nanosecond time scales. The inset shows the millisecond time scales; (b) RF spectrum of mode-locked Nd:$LuVO_4$ laser (first beat note). Inset: the RF spectrum for 1-GHz scan range; The measured autocorrelation trace and output spectrum of a mode-locked Nd:$LuVO_4$ laser for (c) sample 1, and (d) sample 2.

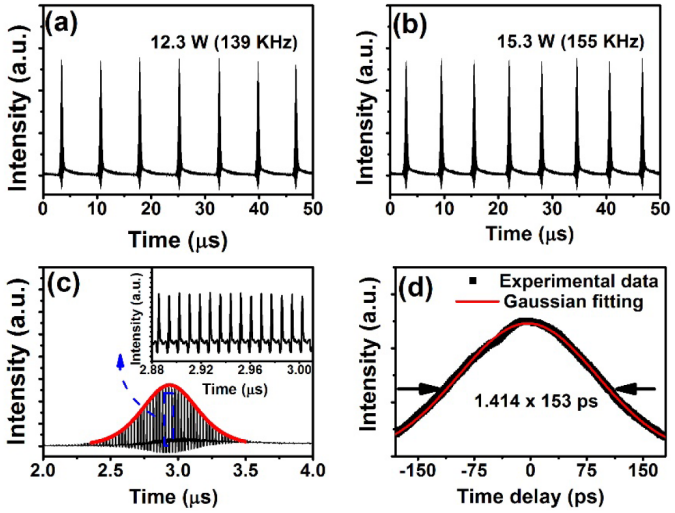

Fig. 7. Time traces of QS-ML pulses at regular state for (a) 139 kHz, and (b) 155 kHz. (c) Expanded temporal shape of a single QS-ML pulse. The inset shows mode-locked pulse trains inside Q-switched envelope. (d) The measured autocorrelation trace (black squares) and curve fitting with Gaussian function (red curve).

5. Conclusion

We have demonstrated stable ML and QS-ML of Nd:$LuVO_4$ laser by using GO films of different transmittance as the SAs. In use of a GOSA with transmittance of 84.1% (ΔT = 2.54%) under 15 W pumping, an Nd:$LuVO_4$ CW mode-locked laser operated at 1065.6 nm with a repetition rate of 121.2 MHz and maximal output power of 3.89 W was obtained. It gives the high pulse energy of 32.14 nJ and peak power of 4.85 kW, which is free from Q-switching modulation. Using GOSA with larger transmittance of 75.9% (ΔT = 4.14%), the narrowest pulse duration of 4.85 ps with 2.73 W output power under pump power of 15 W

Optical Materials EXPRESS

can be achieved. In addition, stable QS-ML state is operated under pumping power of 13.3 to 15.3 W by using the largest transmittance of 63.4% (ΔT = 5.34%) of our sample. Under 15.3 W pump power, the maximal output power of QS-ML, repetition rate, and temporal width of QS envelope is 1.92 W, 155 kHz, and 0.49 μs, respectively. The peak power of QS-ML pulses is 1.18 kW. Our results have demonstrated that GO is a good material for using in high-power DPSSL operated in passively CW-ML and QS-ML states.

Funding

This work is supported by the Ministry of Science and Technology of Taiwan, Republic of China, under grants MOST 103-2221-E-009-106-MY3 and MOST 105-2811-E-009-035.